Available online at www.sciencedirect.com

ScienceDirect

Procedia Engineering 114 (2015) 792 – 799

Procedia Engineering

www.elsevier.com/locate/procedia

1st International Conference on Structural Integrity

Bond-slip effect in the assessment of RC structures subjected to seismic actions

Paulo Silva Lobo[a,b,*], João Almeida[a], Luís Guerreiro[a]

[a]*Department of Civil Engineering, Architecture and Georesources, CEris, Instituto Superior Técnico, University of Lisbon, Av. Rovisco Pais, 1049-001 Lisbon, Portugal*

[b]*Centre of Exact Sciences and Engineering, University of Madeira, Campus Universitário da Penteada, 9000-390 Funchal, Madeira, Portugal*

Abstract

The effect of bond-slip in the assessment of reinforced concrete structures under static or dynamic cyclic loads with numerical models may be significant. Its relevance is discussed in this paper, by analysis of the correlation of experimental and analytical results. The latter were obtained with a perfect bond-based model and with a fiber-section beam-column model which makes it possible to consider the effect of bond-slip in the vicinity of exterior as well of interior joints of reinforced concrete frame structures. The experimental results consist of a shaking table test of a reinforced concrete frame, with predominant flexural condition, in agreement with the premisses of this research. The model with bond-slip was capable of predicting the structural behaviour in a very satisfactory manner. Furthermore, the results of the assessment including bond-slip are significantly more accurate than those assuming perfect bond.

Peer-review under responsibility of INEGI - Institute of Science and Innovation in Mechanical and Industrial Engineering

Keywords: Reinforced concrete; Bond-slip; Fiber-section model; Nonlinear dynamic analysis; Seismic assessment

1. Introduction

Not considering bond-slip and adopting Bernoulli's hypothesis in a reinforced concrete (RC) fiber-section finite element (FE) results in an overestimation of the stiffness of the model, especially relevant near footings and beam-column joints. Also, tension-stiffening is neglected, which, given the damage levels which normally occur in RC structures subjected to extreme cyclic actions, is usually negligible in seismic analysis. Even though they possess the previously mentioned limitations, perfect bond-based models [1] are frequently adopted, mainly due to the simplicity and lower computational effort required. Significant research effort has been put into the development of RC frame element models capable of accounting for bond-slip effects, namely those of the category of fiber-section FEs. In this group there is the model developed by Monti and Spacone [2], obtained from the combination of the fiber beam FE for seismic analysis of RC by Spacone et al. [1] and of the FE for reinforcing bars anchored in concrete of Monti et al. [3]. This formulation makes it possible to account for bond-slip in the end joints of RC frame elements. Also,

* Corresponding author.
E-mail address: paulo.lobo@ist.utl.pt

Peer-review under responsibility of INEGI - Institute of Science and Innovation in Mechanical and Industrial Engineering
doi:10.1016/j.proeng.2015.08.028

the model by Limkatanyiu and Spacone [4], is noted. It allows for the consideration of bond-slip and the coupling effect of adjacent beam-column elements, and consists of a frame element and of a plane rigid-panel joint element. This model leads to the introduction of a significant number of beam FEs to model a structural element. A direct and simple way of considering bond-slip involves implementing nonlinear spring elements at the FE-end nodes [5]. Even though this solution is competitive regarding computational implementation, the constitutive models definition requires *ad-hoc* calibration. Also, the coupling effect of adjacent structural elements cannot be accounted for with these models. D'Amato et al. [6] used the same concept as applied by Monti and Spacone [2] for the implementation of an anchored bar formulation [7] in a concentrated plasticity FE. As in the previous case, this model does not consider coupling effects. Solid models have been proposed [8], but the highly demanding computational implementation currently makes their utilization difficult for the assessment of structures with significant dimensions. A fiber force-based FE with continuous anchored bars was proposed recently [9]. This model makes it possible to consider bond-slip in interior joint regions and, being fiber-section based, accounts for the effect of the variation of the axial force due to the overturning effects on the hysteretic behaviour of the element. The research reported herein makes use of this model and of the model by Monti and Spacone [2] to evaluate the correlation of the predicted response considering bond-slip with experimental results. The relevance of bond-slip is assessed by comparison with the response obtained considering the perfect bond based FE model by Spacone et al. [1].

2. Numerical model for nonlinear dynamic analysis

A FE formulation of a reinforcing bar anchored in concrete with continuous bond was proposed by Monti et al. [3]. The relation $\Delta\mathbf{S} = \mathbf{K}\Delta\mathbf{u}$ between nodal displacements, $\mathbf{u}$, and stresses, $\mathbf{S}$, was presented (a bold symbol is used to represent a vector or a matrix). $\mathbf{K}$ is the stiffness matrix given by the contribution of the rebar element and of the bond forces. Monti and Spacone [2] revised the previous model, making it possible to implement it in a fiber-section FE [1]. The resulting formulation is defined by the anchorage, modelled by a series of n rebar anchored in concrete FEs [3], and the rebar fiber with length L_{IP} (see Fig. 1a). This length should be considered equal to the plastic hinge length of the element [6,9], which may be given by the equation proposed by Bae and Bayrak [10].

The anchorage is assimilated to a spring attached to the rebar fiber, resulting in the anchorage slip law

$$\begin{bmatrix} k_{aa} & \mathbf{k}_{an} \\ \mathbf{k}_{na} & \mathbf{k}_{nn} \end{bmatrix} \begin{Bmatrix} \Delta u_a \\ \Delta \mathbf{u}_n \end{Bmatrix} = \begin{Bmatrix} \Delta\sigma_a \\ \mathbf{0} \end{Bmatrix} \tag{1}$$

where the subscript n refers to the anchorage FEs nodes other than the node of the anchorage/rebar fiber interface, in which case the subscript a is adopted. k_{aa}, $\mathbf{k}_{an}$, $\mathbf{k}_{na}$ and $\mathbf{k}_{nn}$ are terms in the anchored bar stiffness matrix, u refers to the nodal displacements of the anchorage FEs and σ_a is the stress at the anchorage-end, equal to the stress along the rebar fiber, σ_{s+a}, in which the subscript is a reference to steel bar plus anchorage. u_a is equal to $\varepsilon_a L_{IP}$. The anchorage

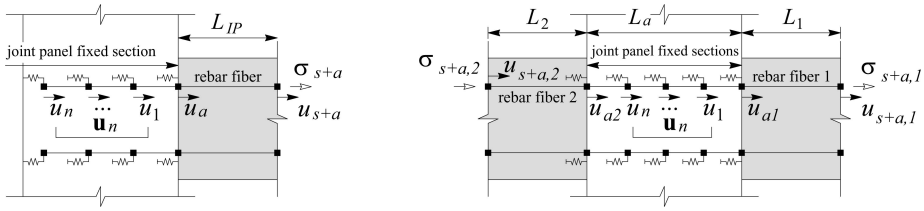

(a) Exterior joint (b) Interior joint

Fig. 1: Anchored rebars with bond-slip in beam column joints; (a) and (b) in the image caption

plus rebar fiber series system may then be described by $(E/L_{IP} \cdot k_a)/(E/L_{IP} + k_a) \cdot \Delta u_{s+a} = \Delta\sigma_{s+a}$, where E is the elasticity modulus of steel and $k_a = k_{aa} - \mathbf{k}_{an}\mathbf{k}_{nn}^{-1}\mathbf{k}_{na}$. The relation between the normal stress and the strain of the fiber is obtained knowing that $u_{s+a} = \varepsilon_{s+a} L_{IP}$, resulting in $E_{s+a}\Delta\varepsilon_{s+a} = \Delta\sigma_{s+a}$. For column-foundation or exterior beam-column joints, the previous formulation can be implemented directly in a fiber-section FE model, such as the one proposed by Spacone et al. [1].

A FE capable of modelling bond-slip in interior joints of RC elements was recently proposed [9]. The model of the continuous anchored rebar with bond-slip, which integrates the mentioned FE, is a generalization of the anchored element formulation addressed previously. It consists of three springs in series (see Fig. 1b), in which the anchorage is modelled by a series of $n + 1$ bars with continuous bond [3]. The anchorage tangent stiffness matrix results in

$$\begin{bmatrix} \mathbf{k}_{a,a} & \mathbf{k}_{a,n} \\ \mathbf{k}_{n,a} & \mathbf{k}_{n,n} \end{bmatrix} \begin{Bmatrix} \Delta\mathbf{u}_a \\ \Delta\mathbf{u}_n \end{Bmatrix} = \begin{Bmatrix} \Delta\boldsymbol{\sigma}_a \\ \mathbf{0} \end{Bmatrix} \tag{2}$$

where $\Delta\mathbf{u}_a = \{\Delta u_{a1}\ \Delta u_{a2}\}^T$ and $\Delta\boldsymbol{\sigma}_a = \{\Delta\sigma_{a1}\ \Delta\sigma_{a2}\}^T$. The 1 and 2 subscripts indicate the rebar fibers on each side of the joint anchorage. With $\mathbf{k}_a = \mathbf{k}_{a,a} - \mathbf{k}_{a,n}\mathbf{k}_{n,n}^{-1}\mathbf{k}_{n,a}$, adding the rebar fibers to the anchorage, yields

$$\begin{bmatrix} \mathbf{k}_{12} & -\mathbf{k}_{12} \\ -\mathbf{k}_{12} & \mathbf{k}_a + \mathbf{k}_{12} \end{bmatrix} \begin{Bmatrix} \Delta\mathbf{u}_{s+a} \\ \Delta\mathbf{u}_a \end{Bmatrix} = \begin{Bmatrix} \Delta\boldsymbol{\sigma}_{s+a} \\ \mathbf{0} \end{Bmatrix} \qquad \text{with} \qquad \mathbf{k}_{12} = \begin{bmatrix} E/L_1 & 0 \\ 0 & E/L_2 \end{bmatrix} \tag{3}$$

where $\Delta\mathbf{u}_{s+a} = \{\Delta u_{s+a,1}\ \Delta u_{s+a,2}\}^T$ and $\Delta\boldsymbol{\sigma}_{s+a} = \{\Delta\sigma_{s+a,1}\ \Delta\sigma_{s+a,2}\}^T$. The previous equation results in $\mathbf{k}_{12}\mathbf{k}_a/(\mathbf{k}_{12} + \mathbf{k}_a) \cdot \Delta\mathbf{u}_{s+a} = \Delta\boldsymbol{\sigma}_{s+a}$. Because the displacements $u_{s+a,1} = \varepsilon_{s+a,1}L_1$ and $u_{s+a,2} = \varepsilon_{s+a,2}L_2$ are obtained at the cross-sections state determination level, the unknowns are the stresses $\sigma_{s+a,1}$ and $\sigma_{s+a,2}$, applied at the rebar fibers-end.

The adopted fiber-section FE is composed of two force-based beam-column elements and three nodes. The interior joint is modelled by the node common to both beam-column FEs, in which the anchored rebar fibers follow the previously addressed model. Furthermore, here the dimensions of the rigid joint are neglected, for simplicity. The constitutive relations of the cross-sections of the three-node element are computed similarly to two-node force-based FEs for $0 \le x_3^{(1)} < L^{(1)}$ and $0 < x_3^{(2)} \le L^{(2)}$, where x_3 is the longitudinal axis of the element, L is the length of the RC elements, and $^{(1)}$ and $^{(2)}$ are references to the elements at each side of the interior joint. For $x_3^{(1)} = L^{(1)}$ and $x_3^{(2)} = 0$, the constitutive relations of both middle-node control-sections cannot be uncoupled, resulting in

$$\begin{Bmatrix} \Delta\mathbf{s}(L)^{(1)} \\ \Delta\mathbf{s}(0)^{(2)} \end{Bmatrix} = \begin{bmatrix} \int_\Omega E^{(1,1)}\mathbf{A}d\Omega & \int_\Omega E^{(1,2)}\mathbf{A}d\Omega \\ \int_\Omega E^{(2,1)}\mathbf{A}d\Omega & \int_\Omega E^{(2,2)}\mathbf{A}d\Omega \end{bmatrix} \begin{Bmatrix} \Delta\mathbf{e}(L)^{(1)} \\ \Delta\mathbf{e}(0)^{(2)} \end{Bmatrix} \tag{4}$$

$\mathbf{s}(x_3) = \{N(x_3)\ M_1(x_3)\ M_2(x_3)\}^T$ is the vector of internal forces at the control-sections, in which M_i is the bending moment about x_i axis. x_1 and x_2 form the axes system of the cross-sections. $\mathbf{e}(x_3) = \{\varepsilon_o(x_3)\,\chi_1(x_3)\,\chi_2(x_3)\}^T$ represents the deformation vector of the cross-sections, in which ε_o is the axial strain at the cross-section coordinate system origin and χ_i is the curvature about x_i. Ω refers to the cross-section domain and $\mathbf{A}$ is composed of terms on x_1 and x_2, making it possible to obtain the stiffness terms of the cross-section. $E^{(1,1)}$ and $E^{(2,2)}$ are the tangent elasticities of the fibers of the cross-sections of the elements $^{(1)}$ and $^{(2)}$, and $E^{(1,2)}$ and $E^{(2,1)}$ are the crossed terms due to the fiber model based on continuous anchored bars, given by adaptation of the equation relating $\Delta\mathbf{u}_{s+a}$ with $\Delta\boldsymbol{\sigma}_{s+a}$, resulting in

$$\begin{bmatrix} E^{(1,1)} & E^{(1,2)} \\ E^{(2,1)} & E^{(2,2)} \end{bmatrix} \begin{Bmatrix} \Delta\varepsilon_{s+a,1} \\ \Delta\varepsilon_{s+a,2} \end{Bmatrix} = \begin{Bmatrix} \Delta\sigma_{s+a,1} \\ \Delta\sigma_{s+a,2} \end{Bmatrix} \tag{5}$$

The equations which relate the independent forces, $\mathbf{q}$, with the internal forces at the cross-sections of each partial element on each side of the interior joint are obtained with an equilibrium transformation matrix, delivering $\Delta\mathbf{s}(x_3) = \bar{\mathbf{B}}\Delta\mathbf{q}$, in which the matrix $\bar{\mathbf{B}}$ contains force-interpolation functions. Substitution of (4), which may include twisting moments, in this equation yields $\{\Delta\mathbf{e}^{(1)}\Delta\mathbf{e}^{(2)}\}^T = \bar{\mathbf{A}}^{-1}\bar{\mathbf{B}} \cdot \{\Delta\mathbf{q}^{(1)}\Delta\mathbf{q}^{(2)}\}^T$, for $x_3^{(1)} = L^{(1)}$ and $x_3^{(2)} = 0$. The tangent flexibility matrix of the three-node FE can be computed with the increments of the independent deformations, $\Delta\mathbf{v}$, defined according to the virtual force principle. Adopting the Gauss-Lobatto integration scheme, with the exception of the control-sections which model the interior joint, the tangent stiffnesses of the cross-sections are determined as usual. In the former case, computation is performed considering the previous equation, delivering

$$\Delta\mathbf{v}^{(1)} = \sum_{i=1}^{n-1} wgt_i L^{(1)}\mathbf{f}_1^{(1)}\Delta\mathbf{q}^{(1)} + wgt_n L^{(1)}\mathbf{f}_2^{(1)} \begin{Bmatrix} \Delta\mathbf{q}^{(1)} \\ \Delta\mathbf{q}^{(2)} \end{Bmatrix} \quad \text{and} \quad \Delta\mathbf{v}^{(2)} = \sum_{i=2}^{n} wgt_i L^{(2)}\mathbf{f}_1^{(2)}\Delta\mathbf{q}^{(2)} + wgt_1 L^{(2)}\mathbf{f}_2^{(2)} \begin{Bmatrix} \Delta\mathbf{q}^{(1)} \\ \Delta\mathbf{q}^{(2)} \end{Bmatrix} \tag{6}$$

in which wgt_i is the ith integration point weight. Adding both equations, results $\{\Delta\mathbf{v}^{(1)}\Delta\mathbf{v}^{(2)}\}^T = \mathbf{f} \cdot \{\Delta\mathbf{q}^{(1)}\Delta\mathbf{q}^{(2)}\}^T$, in which $\mathbf{f}$ is the material flexibility matrix of the three-node FE. The linear compatibility matrix for the adopted FE is

given by $\{\mathbf{v}^{(1)}\ \mathbf{v}^{(2)}\}^T = \mathbf{a}^{(1,2)}\bar{\mathbf{u}}^{(1,2)}$, where $\mathbf{a}^{(1,2)}$ is the compatibility matrix and $\bar{\mathbf{u}}^{(1,2)}$ is the vector of nodal displacements. Any level of geometrical nonlinearity consistent with the small-deformations/large-displacement theory may be added to the model. The analysis reported herein was of the P-Δ type. The element state determination may be computed with a residual displacements based method such as the Spacone et al. [1] method.

3. Correlation of experimental and analytical results

The reference results adopted in this section are the test results of the structure assessed by Clough and Gidwani [11]. These researchers chose to study a structure with predominant flexural conditions, which is in agreement with the conditions also considered in this research. This structure was a model of a typical apartment or office building, built to a length scale of 0.7, consisting of a two-storey, one bay framed structure, with the ground accelerations applied along the direction of the frame. It was designed in order to obtain maximum ductility. With the objective of simulating the mass of a typical building and to obtain representative values of the period of vibration, concrete weights were added to each floor (see Fig. 2a). The construction of two identical, parallel and connected frames allowed the stabilization

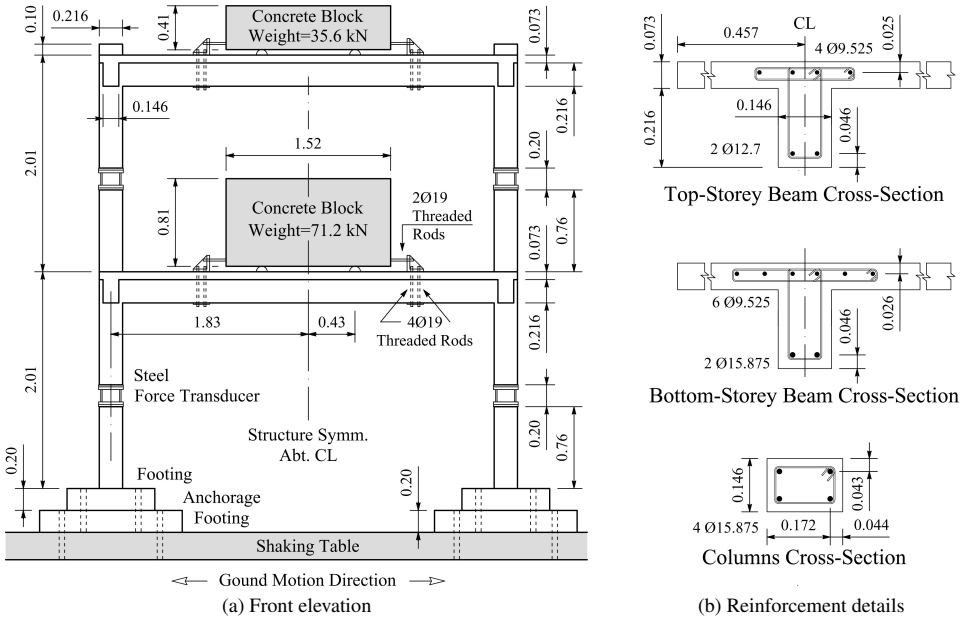

Fig. 2: Geometry, arrangement on shaking table and reinforcement of the test structure (dimensions in meters); (a) and (b) in the image caption

of the direction perpendicular to the ground motion. Also, the inclusion of the slab on the top of the girders allowed the simulation of the flange action conferred by these elements. The rebar detailing is presented in Fig. 2b. The average values of the characteristics of the materials obtained from tests were reported [11]. The reinforcement consists of deformed steel bars with the exception of the rebars used for hoops and stirrups. The relevant values obtained for steel are presented in Table 1. σ_y is the yielding stress, ε_{sh} is the limit strain of the yield plateau, ε_u is the ultimate strain

Table 1: Average test values of the characteristics of the reinforcement bars of the test structure [11].

ϕ (mm)	E (GPa)	σ_y (MPa)	ε_{sh} (‰)	ε_u (‰)	σ_u (MPa)
9.525	195.8	358.5	28.9	193	500.6
12.7	193.1	386.8	17.6	140	578.5
15.875	205.5	286.1	9.4	113	499.9

and σ_u is the ultimate stress. The average values of the unconfined concrete compressive strength, f'_{co} = 30.3 MPa, and of the longitudinal strain at unconfined concrete peak stress, ε_{co} = 3.35‰ , were obtained just before the shaking table test was conducted, with a loading rate of the cylinders of about 0.252 MPa/s.

The ground motion record used is the N69W accelerogram recorded at Taft during the Arvin-Tehachapi earthquake in 1952. The structure was subjected to a low intensity shake, with peak ground acceleration of 9.7% g, with the objective of inducing a normal degree of cracking of common real structures. A second high intensity shake with a peak ground acceleration of 57% g, capable of causing extensive damage, was simulated [11].

Given the structural symmetry, only one frame was numerically assessed. A scheme of the model of the structure is depicted in Fig. 3. The gray squares represent the nodes of the model. Elements 1, 2, 5, 7, 8, 9, 10 and 12 were

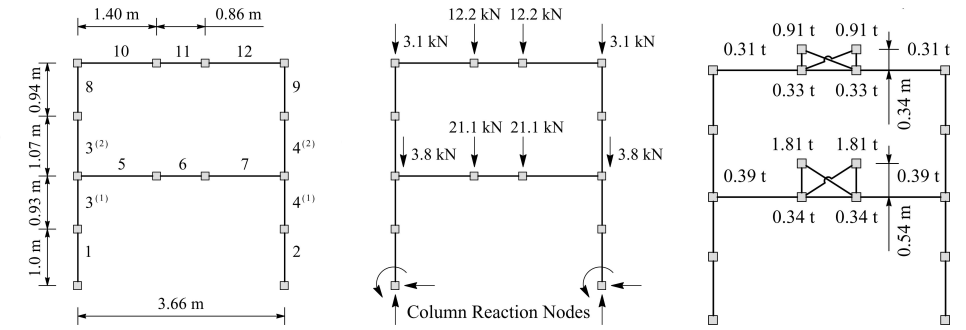

(a) Discretization and geometry (b) Vertical loads and reactions (c) Lumped masses

Fig. 3: Scheme of the model of the test structure; (a), (b) and (c) in the image caption

modelled as two-node FEs with bond-slip in the exterior joints. Elements 3 and 4 are three-node FEs with bond-slip in the interior beam-column joints. Elements 6 and 11 are fiber-section force-based FEs with perfect bond. The bottom column-ends at the footings were considered to be fixed and the columns and girders axis were considered at the centroid of the gross concrete cross-sections. The loads due to the weight of the elements were lumped together with the loads due to the added concrete masses and at the girders exterior nodes. The mass due to self-weight was lumped at the corresponding nodes and, as visible in Fig. 3c, elements were added to allow the allocation of the concrete block masses at their real position. The added trusses, which modelled the support conditions of the concrete blocks, are composed of massless linear elastic elements with high axial stiffness, pinned at both their ends. The beams and columns were simulated with four control-sections for each beam-column, defined according to the Gauss-Lobatto integration scheme. In the case of the three-node FEs, a total of eight control sections per element was considered. All rebars pertaining to exterior joints were modelled following the Monti and Spacone model [2] and for the interior joints the continuous anchored bar fiber model [9] was considered. The concrete cross-sections were discretized into fibers, following the Gauss-Lobatto scheme. In the case of the columns, 10 integration points were considered, and regarding the beams, the flange was modelled with five control points and the web with 10 fibers.

The Monti and Nuti [12] model was considered for steel. For the column rebars, the kinematic strain hardening ratio was taken equal to 0.035 , while for the girder rebars a negligible value fo this parameter was assumed. The model by Martínez-Rueda and Elnashai [13] was used for concrete and the concrete tensile strength was neglected. The confined concrete properties, according to the work by Mander et al. [14], were considered for the fibers inside the hoops. Moreover, the average strain rate of the cylinder tests previously mentioned was close to the quasi-static strength. As such, the dynamic values of strength, elastic modulus and strain at peak stress were obtained considering a strain rate of 1.67×10^{-2} s^{-1} [14]. Bond-slip was modelled following the Eligehausen et al. proposal [15], with constants obtained with the empirical formulas developed by Monti et al. [16]. Hooked bars bond-slip was modelled following the proposal by Eligehausen et al. [17]. All anchorages, either interior or exterior, where modelled with five FEs, with four Gauss-Lobatto integration points for every FE.

Because the nonlinear material behaviour is modelled according to the materials constitutive relations, and because for structures with highly nonlinear response viscous damping is of small importance when compared to hysteretic damping, in this analysis Rayleigh damping was considered, for numerical stability sake, with a negligible value, ζ = 0.1%, for the first two natural vibration modes, with α_M and α_K determined for the frequency values 3.13 and

8.70 Hz measured in the reported snap tests [11]. For the numerical integration of the equations of motion, the Hilber, Hughes and Taylor α-method was used with $\alpha = -0.05$. A time step $\Delta t = 0.005$ s was adopted.

The perfect bond frame model was developed with the exact same characteristics of the bond-slip numerical model described above, using the fiber beam FE for seismic analysis of RC by Spacone et al. [1].

The correlation between the results of the model previously described and the experimental results was made in terms of bottom-storey and top-storey displacements. For evaluation of the influence of bond-slip, the results of the analysis of the model with perfect bond are also presented. The bottom-storey and top-storey displacements comparison with experimental results are depicted in Fig. 4 and 5. Good agreement between experimental and

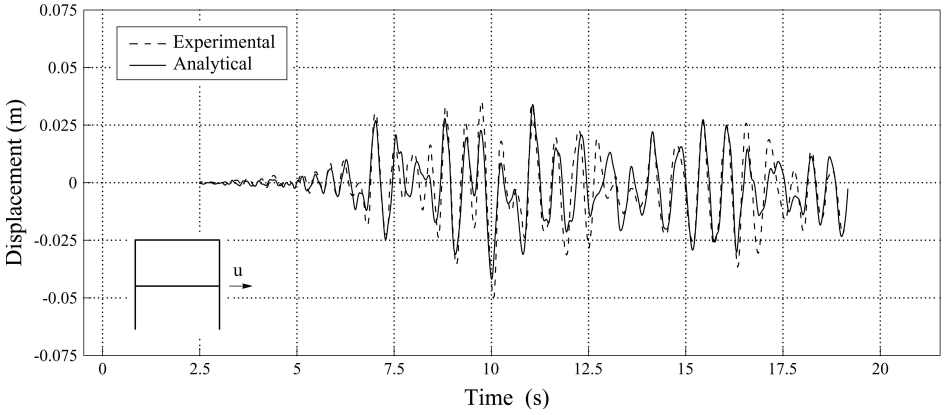

Fig. 4: Correlation of the bottom-storey displacement response of the test structure

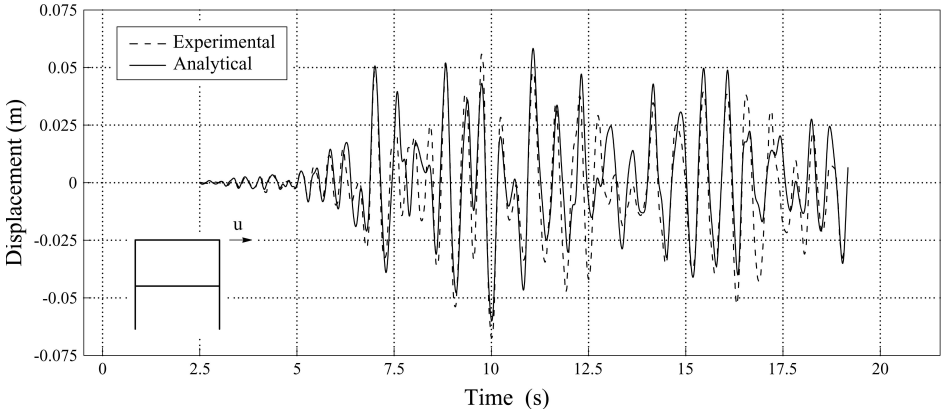

Fig. 5: Correlation of the top-storey displacement response of the test structure

analytical results can be seen. The period of vibration and the waveform obtained with the numerical model correlate well with the test results. Also, the prediction of peak-displacements is very satisfactory.

For evaluation of the effect of bond-slip on the response, the displacements obtained with the models with and without bond-slip are depicted in Fig. 6 and 7. The results of the model without bond-slip correspond in general to smaller displacements and the results present a significantly inferior correlation with the experimental data. Thus, the influence of bond-slip is significant and its consideration made it possible to obtain a significantly better response prediction.

For further analysis of the results, the shear-displacement relation with and without bond-slip of the left column of the bottom-storey are depicted in Fig. 8. As expected, the energy dissipation obtained with the consideration of perfect bond is significantly higher than that of the more sophisticated model, including rebars bond-slip behaviour.

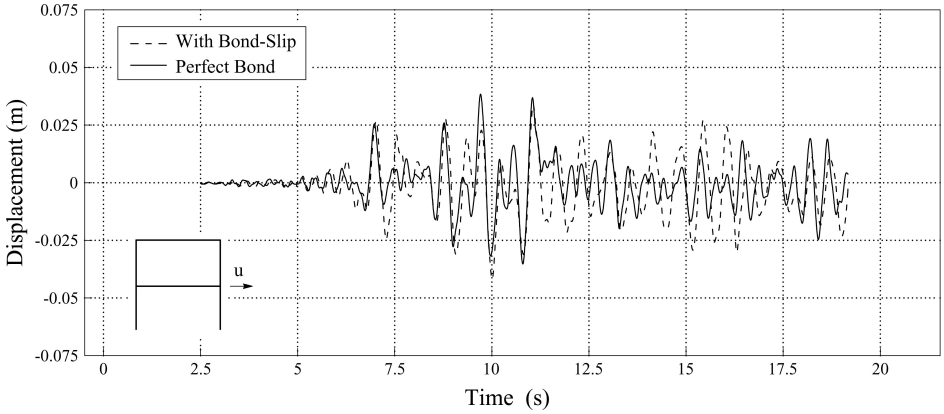

Fig. 6: Bond-slip effect on the bottom-storey displacement response of the test structure

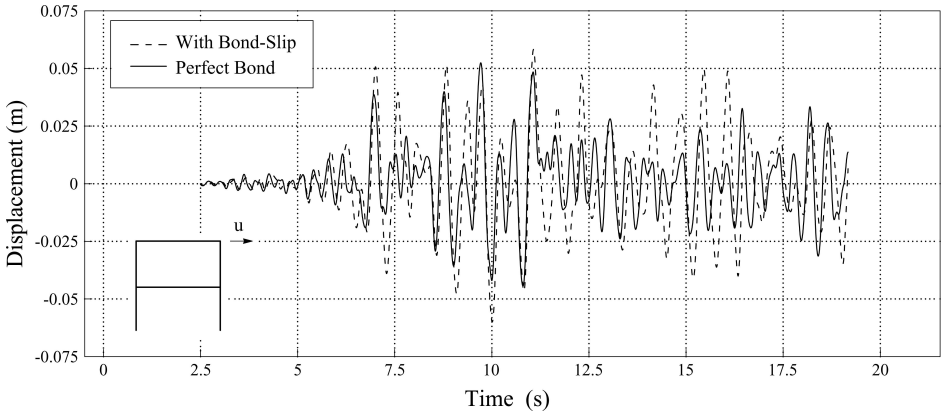

Fig. 7: Bond-slip effect on the top-storey displacement response of the test structure

The markedly more pinched response of the bond-slip model is noted, consistent with the results for static cyclic loads of the applied models previously reported [2,9]

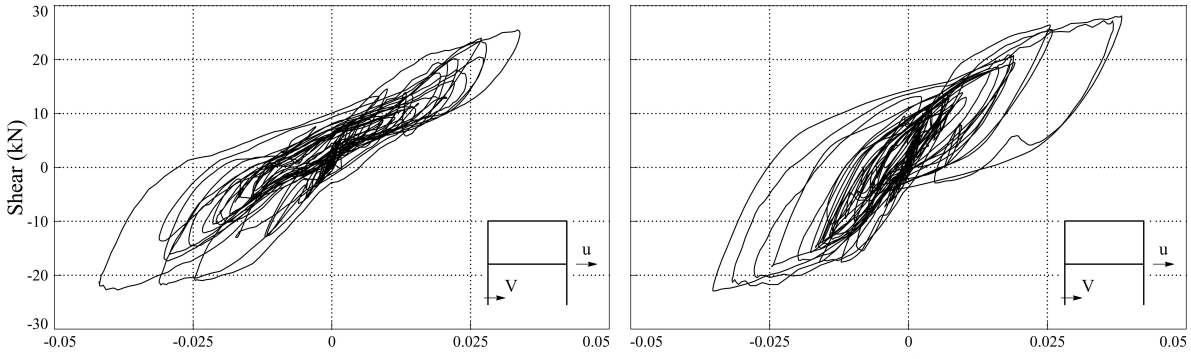

(a) With bond-slip (b) Perfect bond

Fig. 8: Analytical bottom-storey shear-displacement relation of the left-side column of the test structure; (a) and (b) in the image caption

4. Conclusions

Fiber-section models for nonlinear analysis of structures subjected to strong cyclic actions were used to assess the response of a RC structure. The objective of this research was to evaluate the effect of bond-slip in the prediction of the response of RC frame structures, thus two models were considered: a frame FE model considering perfect bond and a model considering bond-slip in both exterior and interior joint regions. The numerical analyses performed are of the nonlinear dynamic type, considering nonlinear geometric and material behaviour, and the reference results adopted are from a shaking table test of a two-storey RC frame structure. As the correlation of experimental and analytical results show, the model with bond-slip in the vicinity of interior and exterior joints is capable of predicting the structural behaviour of RC frame structures subjected to dynamic loads in a very satisfactory manner. It is stressed that the model was developed based only on the reported material and geometric properties of the reference test frame, without any calibration procedures. The influence of bond-slip on the response was also assessed by comparison of the results of the more sophisticated model with the results of the model with perfect bond. This comparison makes it possible to conclude that the model with bond-slip is significantly more accurate than the model with perfect bond. Also, the response in terms of shear-storey displacement was assessed, showing that the pinching effect in the hysteretic cycles, an effect which is observable in experimental tests of RC structures and that has significant influence on the overall structural response as it reduces the energy dissipated, is noticeable in the response obtained with the bond-slip model, unlike for the perfect bond model. The numerical model robustness and efficiency, as well as accuracy, was shown with the assessed example, adding to previously reported applications.

References

[1] E. Spacone, F. C. Filippou, F. F. Taucer, Fibre beam-column model for non-linear analysis of R/C frames: Part I. Formulation, Earthquake Engineering and Structural Dynamics 25 (7) (1996) 711–725, doi:10.1002/(SICI)1096-9845(199607)25:7<711::AID-EQE576>3.0.CO;2-9.

[2] G. Monti, E. Spacone, Reinforced concrete fiber beam element with bond-slip, J. Struct. Engrg., ASCE 126 (6) (2000) 654–661, doi:10.1061/(ASCE)0733-9445(2000)126:6(654).

[3] G. Monti, E. Spacone, F. C. Filippou, Model for anchored reinforcing bars under seismic excitations, Tech. Rep. UCB/EERC-93/08, Earthquake Engineering Research Center, College of Engineering, University of California, Berkeley, California (December 1993).

[4] S. Limkatanyu, E. Spacone, Effects of reinforcement slippage on the non-linear response under cyclic loadings of RC frame structures, Earthquake Engineering and Structural Dynamics 32 (15) (2003) 2407–2424, doi:10.1002/eqe.334.

[5] N. R. Rubiano-Benavides, Prediction of the inelastic seismic response of concrete structures including shear deformations and anchorage slip, Doctoral dissertation, University of Texas, Austin, Texas (1998).

[6] M. D'Amato, F. Braga, R. Gigliotti, S. Kunnath, M. Laterza, Validation of a modified steel bar model incorporating bond-slip for seismic assessment of concrete structures, Journal of Structural Engineering 138 (11) (2012) 1351–1360. doi:10.1061/(ASCE)ST.1943-541X.0000588.

[7] F. Braga, R. Gigliotti, M. Laterza, M. DAmato, S. Kunnath, Modified steel bar model incorporating bond-slip for seismic assessment of concrete structures, Journal of Structural Engineering 138 (11) (2012) 1342–1350. doi:10.1061/(ASCE)ST.1943-541X.0000587.

[8] H. G. Kwak, F. C. Filippou, A new reinforcing steel model with bond-slip, Struct. Eng. Mech. Int. J. 3 (4) (1995) 299–312, doi:10.1002/eqe.334.

[9] P. Silva Lobo, J. Almeida, RC fiber beam-column model with bond-slip in the vicinity of interior joints, Engineering Structures 96 (0) (2015) 78–87. doi:10.1016/j.engstruct.2015.04.005.

[10] S. Bae, O. Bayrak, Plastic hinge length of reinforced concrete columns, ACI Structural Journal 105 (3) (2008) 290–300, doi:10.14359/19788.

[11] R. W. Clough, J. Gidwani, Reinforced concrete frame 2: Seismic testing and analytical correlation, Tech. Rep. EERC-76/15, Earthquake Engineering Research Center, College of Engineering, University of California, Berkeley, California (June 1976).

[12] G. Monti, C. Nuti, Nonlinear cyclic behavior of reinforcing bars including buckling, J. Struct. Engrg., ASCE 118 (12) (1992) 3268–3284, doi:10.1061/(ASCE)0733-9445(1992)118:12(3268).

[13] J. E. Martínez-Rueda, A. S. Elnashai, Confined concrete model under cyclic load, Materials and Structures 30 (1997) 139–147, doi:10.1007/BF02486385.

[14] J. B. Mander, M. J. N. Priestley, R. Park, Theoretical stress-strain model for confined concrete, J. Struct. Engrg., ASCE 114 (8) (1988) 1804–1826, doi:10.1061/(ASCE)0733-9445(1988)114:8(1804).

[15] R. Eligehausen, E. P. Popov, V. V. Bertero, Local bond stress-slip relationships of deformed bars under generalized excitations, Tech. Rep. UCB/EERC-83/23, Earthquake Engineering Research Center, College of Engineering, University of California, Berkeley, California (October 1983).

[16] G. Monti, A. De Sortis, C. Nuti, Problemi di scala nella sperimentazione pseudodinamica di pile da ponte in C.A., in: Workshop Danneggiamento, Prove Cicliche e Pseudodinamica, Napoli, Italy, 1994.

[17] R. Eligehausen, V. V. Bertero, E. P. Popov, Hysteretic behavior of reinforcing deformed hooked bars in R/C joints, in: 7th Eur. Conf. on Earthquake Engrg., Vol. 4, Technical Chamber of Greece, Athens, 1982, pp. 171–178.